Computational Materials Science 210 (2022) 111050

Contents lists available at ScienceDirect

Computational Materials Science

journal homepage: www.elsevier.com/locate/commatsci

First-principles analysis of the grain boundary segregation of transition metal alloying elements in γFe

Kazuma Ito *, Hideaki Sawada

Advanced Technology Research Laboratories, Nippon Steel Corporation, 20-1 Shintomi, Futtsu-city, Chiba 293-8511, Japan

ARTICLE INFO

Keywords:
Ab initio calculation
Grain boundaries
Segregation
Steel

ABSTRACT

In this study, first-principles calculations were carried out for the first time to systematically investigate the grain boundary segregation of transition metal alloying elements (Ti, V, Cr, Mn, Co, Ni, Cu, Nb, and Mo) in paramagnetic γFe and its dependence on the grain boundary character. The segregation energies of each element and site were comprehensively calculated for nine [0 0 1] symmetric tilt grain boundary models with Σ values from 5 to 41; the paramagnetic state was simulated by the antiferromagnetic double-layer (AFMD). By calculating the effective segregation energy for each grain boundary model from the obtained segregation energies, the grain boundary segregation behavior for each alloying element and its dependence on the grain boundary character were investigated. The segregation energy of transition metal elements is dominated by the Voronoi volume of Fe at the segregation site and arises from the elastic energy derived from the difference in atomic radii between the host and solute metals. Ti, Cu, Nb, and Mo have negative effective segregation energies (indicating a tendency toward segregation) at all investigated grain boundaries, and the absolute values of the effective segregation energy increase in the order of Cu < Mo < Ti < Nb in all of the grain boundary models. In contrast, the sign of the effective segregation energies for V, Ni, and Co changes depending on the grain boundary, and the effective segregation energies for Cr and Mn are positive at all grain boundaries. These results corresponded well with the experimental results. The results obtained in this study provide important basic data for the material design of high-strength steels and are useful for understanding the effects of alloying elements in γFe.

1. Introduction

Steel is a widely used and important structural material. In recent years, the demand for high-strength steel, especially for automotive steel sheets, has been increasing, and research and development of such steel has also increased [1–6]. However, in general, as the material strength increases, the susceptibility to hydrogen embrittlement also increases [7–9], limiting its application.

For example, in martensitic high-strength steels, cracking at the prior γ grain boundary in a hydrogen environment is a serious problem [5,10,11]. It has been shown that grain boundary cracking in hydrogen environments is closely related to the grain boundary segregation of alloying elements at the prior γ grain boundaries. Because the grain boundary segregation state at the prior γ grain boundary is mainly determined in the γ region, controlling the grain boundary segregation in the γ region is important for improving the hydrogen embrittlement resistance of martensitic high-strength steels. To control the grain boundary segregation, it is necessary to obtain basic data on the grain boundary segregation tendency of each alloying element and its dependence on the grain boundary character. In addition, because various impurities and alloying elements are included in practical steels, it is important to clarify the physical origin of grain boundary segregation to understand the effects of these impurities. However, because γFe is a stable phase at high temperatures, there is little experimental data on the grain boundary segregation of various alloying elements at grain boundaries [12].

First-principles calculations have been shown to be effective for the analysis of grain boundary segregation. In particular, many studies have been conducted on the grain boundary segregation of alloying and impurity elements in αFe, and it has been reported that the segregation energy of solute elements obtained by first-principles calculations can semi-quantitatively reproduce the experimentally obtained segregation energy in polycrystalline grain boundaries [13–23]. These calculations have also been shown to be effective for clarifying the physical origin of grain boundary segregation [18,20,21]. On the other hand, few studies have analyzed the grain boundary segregation in γFe owing to the

* Corresponding author.
E-mail address: ito.nn3.kazuma@jp.nipponsteel.com (K. Ito).

https://doi.org/10.1016/j.commatsci.2021.111050
Received 10 August 2021; Received in revised form 7 November 2021; Accepted 12 November 2021
Available online 24 November 2021

difficulty of handling paramagnetism in first-principles calculations [24]. As a result, there is insufficient knowledge to control the above-mentioned grain boundary segregation.

In this study, we propose a magnetic state and data set of grain boundary models for the systematic investigation of grain boundary segregation in paramagnetic γFe through first-principles calculations. The segregation energies of nine transition metal alloying elements (Ti, V, Cr, Mn, Co, Ni, Cu, Nb, and Mo) commonly used in steel materials are calculated. From the obtained segregation energies, the effective segregation energies in each grain boundary model are calculated to investigate the grain boundary segregation tendency of each alloying element and its dependence on the grain boundary character. For some elements for which comparable experimental results exist, the validity of the calculation results is verified by comparing with the experimental results. Based on the phenomenological model of grain boundary segregation, the physical origin of the grain boundary segregation of transition metal elements in γFe is also discussed.

2. Calculation method

2.1. Magnetic structure to simulate paramagnetism and data set for the grain boundary model

Magnetic structures that assign a positive or negative magnetic moment to each Fe atom based on special quasi-random structures (SQSs) [25] have been shown to be effective for the calculation of solute elements in bulk γFe [26]. However, the SQS algorithm cannot be directly applied to grain boundaries. In this study, we used the antiferromagnetic double-layer (AFMD) [27,28] state to simulate the magnetic state of the paramagnetic bulk γFe and grain boundaries. The magnetic structure of the AFMD has been shown to be the most energetically stable among γFe with a collinear magnetic structure [29]. The lattice parameter of γFe in the AFMD magnetic structure is similar to that of paramagnetic γFe [29]. In addition, the electronic states of solute atoms in γFe in the AFMD magnetic structure are similar to those in the magnetic structure using SQSs [24]. The validity of using the AFMD magnetic structure is discussed further based on the calculation results in Section 3.

The data set of grain boundary models, including [0 0 1] symmetric tilt grain boundaries, were used to analyze the grain boundary segregation. As described below, the use of [0 0 1] symmetric tilt grain boundaries with the AFMD state allows the total magnetic moment in the grain boundary model to be zero. Furthermore, the good symmetry of [0 0 1] symmetric tilt grain boundaries greatly reduces the computational cost of determining the effective segregation energy. The grain boundary models were selected and constructed considering the calculation accuracy and calculation cost for the structural relaxation of the grain boundary model and segregation energy. The initial structure of the grain boundary model was created using the data set of the stable grain boundary structure of the [0 0 1] symmetric tilt angle grain boundary of Cu proposed by Tschopp et al. [30]. These grain boundary structures of Cu were scaled by the lattice constant of γFe in the AFMD magnetic structure, and were used as candidates for the initial structure [30]. The thus-obtained grain boundary structure had good transferability as an initial structure to obtain stable grain boundaries of other fcc metals. The candidate initial structure was created as a slab model by extracting the atomic structure, including the grain boundary, to remove the restriction associated with the periodic boundary condition in the direction perpendicular to the grain boundary. The cell size in the [0 0 1] direction was set to 7.08 Å, which is the unit cell size of γFe in the AFMD magnetic structure. The cell size in the axis perpendicular to the [0 0 1] direction and parallel to the grain boundary plane was also set to at least 7.08 Å to reduce the interaction between solute elements due to the periodic boundary condition. Under these conditions, we searched for grain boundary models including all [0 0 1] symmetric tilt grain boundaries that could be constructed with fewer than 300 atoms. Some methods have been proposed to search for stable grain boundary structures, for example, the γ-surface approach method in which two slabs with different crystal orientations are shifted [31], and a method based on evolutionary algorithms that performs an efficient grand-canonical grain boundary structure search [32]. These methods cannot be used in this study because of the computational cost associated with the number of atoms and the instability of the spin-polarized electronic structure calculation in the grain boundary model. However, note that for the purpose of this study, the grain boundary structure employed does not necessarily have to be the most stable grain boundary structure at the corresponding grain boundary character and orientation difference.

Fig. 1 shows the atomic structures of the obtained grain boundary models. Table 1 lists the tilt angle, Σ value, and grain boundary energy of the grain boundaries in each model. A variety of grain boundary models were obtained with tilt angles ranging from 18.9° to 77.3°, Σ values ranging from 5 to 41, and grain boundary energies ranging from 0.81 to 1.33 J/m^2. Fig. 2 shows the magnetic moment of each Fe atom in the Σ5 (3 1 0) grain boundary model as an example. Near the center of the grain boundary, the magnetic moment varies with the distance from the grain boundary center owing to the magnetovolume effect, but the total magnetic moment of the grain boundary model can be reduced to zero for the [0 0 1] symmetric tilt grain boundaries. In Fig. 1, the region within 2.5 Å from the grain boundary center of each grain boundary model analyzed in this study is indicated by a dotted line. The sites included in this region are referred to as grain boundary sites. The reason for choosing 2.5 Å here is to efficiently select sites that strongly reflect the influence of each grain boundary character. It is known that the grain boundary diffusion of solute elements in Cu is well explained by setting the segregation zone to 2.5 Å from the center of the grain boundary (5.0 Å for the grain boundary width) [33,34]. Furthermore, when experimentally evaluating grain boundary segregation at αFe grain boundaries, it is typical to consider the segregation area as within 2.5 Å, which is one atomic diameter of αFe, from the center of the grain boundary [35,36]. We also found that grain boundary segregation is particularly pronounced within 2.5 Å from the center of the grain boundary, based on an exhaustive calculation of the segregation energy of P using the interatomic potential at grain boundaries in αFe polycrystals [37,38]. The main segregation area in γFe is expected to be comparable to that of αFe and Cu; therefore, 2.5 Å was selected.

It is necessary to obtain the segregation energy for all inequivalent grain boundary sites to calculate the effective segregation energy for

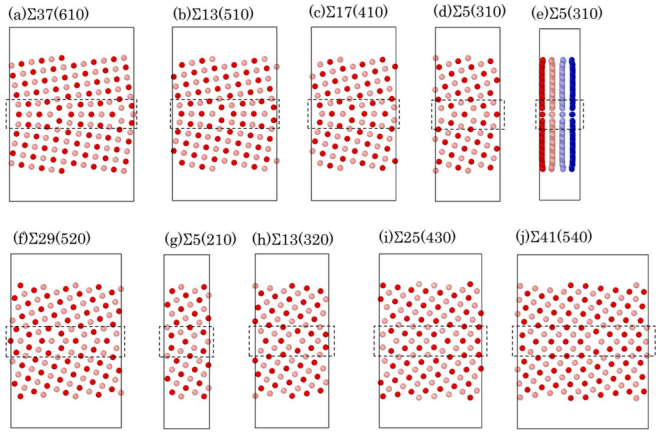

Fig. 1. Grain boundary character and atomic structure for each grain boundary model. The region within 2.5 Å from the center of the grain boundary is indicated by the dotted lines. The color of each atom represents the coordinate in the [0 0 1] axis direction. Red or pink atoms have positive magnetic moments, and blue or light blue atoms have negative magnetic moments; (e) shows the atomic structure of the Σ5(3 1 0) grain boundary model in (d) viewed from the [1 3 0] direction.

Table 1
Properties of the grain boundary models. The grain boundary character, misorientation angle, grain boundary energy, and cell dimensions of each grain boundary model are listed. The number of atoms and inequivalent segregation sites in each grain boundary model are also given.

Grain boundary	Misorientation angles (degrees)	Number of atoms in grain boundary model	Number of inequivalent grain boundary sites	Cell dimensions (Å)	Grain boundary energy (J/m^2)
Σ37(610)	18.9	276	11	21.53 × 7.08 × 30.00	1.07
Σ13(510)	22.6	224	9	18.05 × 7.08 × 30.00	1.13
Σ17(410)	28.1	180	7	14.60 × 7.08 × 30.00	1.20
Σ5(310)	36.9	144	5	11.19 × 7.08 × 30.00	1.24
Σ29(520)	43.6	240	9	19.06 × 7.08 × 30.00	1.29
Σ5(210)	53.1	100	4	7.92 × 7.08 × 30.00	1.33
Σ13(320)	67.4	160	6	12.76 × 7.08 × 30.00	1.08
Σ25(430)	73.7	228	9	17.70 × 7.08 × 30.00	0.91
Σ41(540)	77.3	288	12	22.67 × 7.08 × 30.00	0.81

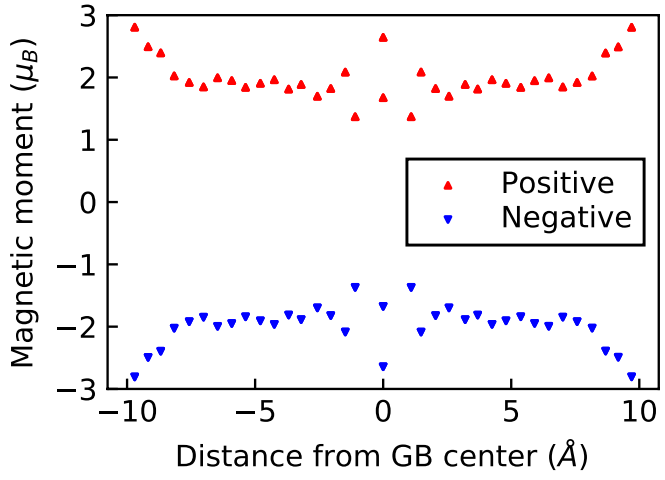

Fig. 2. Magnetic moments of each atom in the Σ5(310) symmetric tilt grain boundary model. The red and blue dots correspond to the magnetic moments of the atoms with positive and negative initial magnetic moments, respectively.

each grain boundary model, as described in the next section. Because of the highly symmetric magnetic structure of the [001] symmetric tilt grain boundaries, the number of inequivalent sites can be significantly reduced, as indicated in Table 1. Note that the magnetic structure of the AFMD was not necessarily the most stable magnetic state in these grain boundary models. However, the magnetic structure of the AFMD, which was given as the initial magnetic moment, was maintained in all the grain boundary models calculated in this study, indicating the high stability of the magnetic structure of the AFMD.

2.2. Details of the first-principles calculations

The spin-polarized electronic structure calculations and structural optimization for the segregation energy calculations were performed using the Vienna ab initio simulation package (VASP) with projector-augmented wave potentials [39,40]. The exchange–correlation effects were treated in the framework of the generalized gradient approximation (GGA) using the Perdew–Burke–Ernzerhof parametrization [41]. The cutoff energy for the plane-wave basis set was 350 eV. The Brillouin zone integration was sampled using a k-spacing of 0.3 $Å^{-1}$ based on the Monkhorst–Pack scheme [42]. The Methfessel–Paxton smearing method [32] with a 0.2 eV width was used. The lattice parameter and magnetic moment of γFe obtained under these conditions were 3.54 Å and 1.93 μ_B, respectively, which are in good agreement with previous studies [24,43]. For Nb, which had the largest segregation energy, calculations were performed by varying the cutoff energy and k-point spacing, and it was confirmed that the grain boundary segregation energy converged in the range of 0.01 eV under the above conditions.

The grain boundary calculations were based on the grain boundary models presented in Fig. 1 and Table 1. To calculate the bulk γFe, which serves as the energy reference for the segregation energy in each grain boundary model, a slab model without grain boundaries but having the same cell size and number of atoms as each grain boundary model was used. The atomic positions were relaxed until the energy convergence was 10^{-4} eV, and the force convergence was 10^{-2} eV/Å. For the grain boundary and bulk calculations without a solute element, all of the atoms were relaxed. Structural relaxation of the grain boundary and bulk models with solute elements was carried out by fixing only the atoms located less than 2 Å from the surfaces in the structures obtained by structural relaxation of the grain boundary and bulk models without solute elements.

2.3. Calculation methods for the grain boundary segregation energy and effective grain boundary segregation energy

The grain boundary segregation energy was calculated for all inequivalent substitutional sites located less than 2.5 Å from the grain boundary center for each grain boundary model. Note that the atomic volumes of the solute elements other than Ni calculated in this study are larger than the atomic volume of γFe (11.1 $Å^3$) under the AFMD magnetic state, and the atomic volume of Ni (11.0 $Å^3$) is comparable to that of γFe. The number of inequivalent sites in each grain boundary model is given in Table 1. The grain boundary segregation energy, E^i_{seg}, for site i was evaluated using the following equation:

$$E^i_{seg} = \left(E^i_{gb}[1\mathrm{X},(N-1)] - E_{gb}[N\mathrm{Fe}]\right) - \left(E_{bulk}[1\mathrm{X},(M-1)\mathrm{Fe}] - E_{bulk}[M\mathrm{Fe}]\right) \quad (1)$$

Note that larger negative values are defined here to indicate a higher segregation tendency at site i. $E_{gb}[N\mathrm{Fe}]$ is the total energy of the grain boundary model without a solute element consisting of N Fe atoms. $E^i_{gb}[1\mathrm{X},(N-1)]$ is the total energy of the grain boundary model containing $N-1$ Fe atoms with one solute element, X, present at site i. $E_{bulk}[M\mathrm{Fe}]$ is the total energy of the bulk model consisting of M Fe atoms. $E_{bulk}[1\mathrm{X},(M-1)\mathrm{Fe}]$ is the total energy of the bulk model containing one

solute element and $M-1$ Fe atoms. Here, M and N are equal, and the value of N for each grain boundary model is given in Table 1.

To evaluate the grain boundary segregation tendency of alloying elements at each grain boundary, the effective segregation energy [44] of each grain boundary model was calculated from the obtained segregation energy for each site. The amount of segregation of the solute in the region within 2.5 Å from the grain boundary center of each grain boundary model can be calculated using the Coghlan–White equation [45], which is an extension of Mclean's equation [46], considering the site dependence of the segregation energy, as follows:

$$c_{gb} = \sum_i \left(F_i c^i_{gb} \right) \tag{2}$$

where F_i is the ratio of sites with segregation energy E^i_{seg} to all grain boundary sites in the region within 2.5 Å from the center of the grain boundary, and c^i_{gb} is the probability of the presence of the solute element at site i with a grain boundary segregation energy of E^i_{seg}. c^i_{gb} was calculated as follows:

$$c^i_{gb} = \frac{c_{bulk} exp\left(-\frac{E^i_{seg}}{k_B T} \right)}{1 - c_{bulk} + c_{bulk} exp\left(-\frac{E^i_{seg}}{k_B T} \right)} \tag{3}$$

where k_B is the Boltzmann constant, T is the temperature, and c_{bulk} is the bulk composition of the solute element.

The effective segregation energy, E^{eff}_{seg}, is defined as follows using c_{gb}:

$$E^{eff}_{seg} = -k_B T \ln \left(\frac{c_{gb}(1 - c_{bulk})}{c_{bulk}(1 - c_{gb})} \right) \tag{4}$$

To evaluate the grain boundary segregation tendency of the alloying elements at each grain boundary, E^{eff}_{seg} of the alloying elements was calculated for $c_{bulk} = 0.0001$ (0.01 at.%) at $T = 1173$ K using equations (2), (3), and (4). Here, c_{bulk} was set to 0.01 at.% as the bulk composition where strong carbide-forming elements such as Nb and Ti can remain in the solid solution even in the presence of C. The resulting E^{eff}_{seg} is the effective segregation energy that considers the segregation energy of each grain boundary site in each grain boundary model. This was used to evaluate the grain boundary segregation tendency of the alloying elements at each grain boundary. For some alloying elements with comparable (existing) experimental results exist, the effective segregation energies were calculated under conditions corresponding to the experimental conditions, and the validity of the calculation method was investigated by comparison with the experimental results.

3. Results and discussion

3.1. Grain boundary segregation energy and its physical origin

Fig. 3 shows the relationship between the segregation energy and the Voronoi volume of Fe at the grain boundary without a solute element at the segregation site calculated using nine grain boundary models for each element. It can be seen that there is a good correlation between the segregation energy and the Voronoi volume for all elements. For Ti, V, Cu, Nb, and Mo, the segregation energy is negatively higher at sites where the Voronoi volume is larger than that of the bulk, while the segregation energy is positive at sites where the Voronoi volume is smaller than that of the bulk. The dependence on the Voronoi volume increases in the order of Cu < V < Mo < Ti < Nb. For Ni and Co, the segregation energy tends to become slightly positive as the Voronoi volume increases. In the case of Cr, the segregation energy is almost independent of the Voronoi volume and has small positive values at many sites. For Mn, the segregation energy also has small positive values

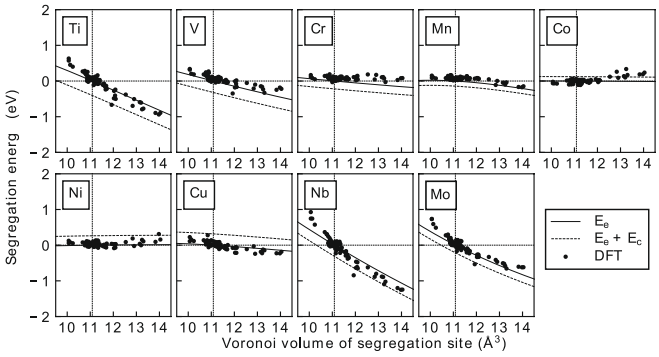

Fig. 3. Relationship between the segregation energy and the Voronoi volume of Fe at the segregation site. The dots indicate the segregation energies obtained by first-principles calculations. The solid line represents the elastic contribution to the segregation energy in the phenomenological model (Eq. (5)). The dashed line is the sum of the elastic and chemical contributions in the phenomenological model (Eqs. (5) and (6)). The vertical dotted line represents the Voronoi volume of Fe in the γFe bulk.

at many sites, but it has small negative values only at sites with particularly large Voronoi volumes.

Fig. 4 shows histograms of the segregation energy for each element calculated using the nine grain boundary models. The larger the dependence of the segregation energy on the Voronoi volume, the larger is the variance in the segregation energy. For example, Nb, which has the largest dependence on the segregation energy, shows a dispersion in the range of −1.25 eV to 0.92 eV. On the other hand, for Cr, where the dependence is small, the dispersion is also small and the segregation energy is localized near zero. This behavior arises because there are many sites near the grain boundary where the Voronoi volume differs from that of the bulk, and the larger the dependence of the Voronoi volume on the segregation energy of each element, the larger the change in the segregation energy. The results of the segregation energy calculations are summarized in Table S1.

To investigate the physical origin of the grain boundary segregation of each element, we calculated the dependence of the grain boundary segregation energy of each element on the Voronoi volume of the segregation site based on the phenomenological model of grain boundary segregation. The main contributions to grain boundary segregation were clarified by comparing the results with those obtained by first-principles calculations. The contributions to the grain boundary segregation energy generally comprise chemical and elastic contributions in the phenomenological model. The former is related to the difference in the cohesive energy between the solute element and the host metal, while the latter is related to the difference in atomic size between the solute element and the host metal. The chemical contribution to the segregation energy, E^c_{seg}, is often evaluated using the following equation [47–49]

$$E^c_{seg} = C(E_c[BinA] - E_c[A]) \tag{5}$$

It should be noted that the larger the negative value, the greater the chemical contribution is to promoting segregation. Here, $E_c[A]$ is the cohesive energy of the host metal, and $E_c[BinA]$ is the cohesive energy of the solute element in the host metal. The constant C is related to the change in the number of bonds between the bulk and grain boundary. This equation indicates that solutes with a small cohesive energy tend to segregate at the grain boundaries. In Eq. (5), within the Friedel model [50], $E_c[A]$ is given by $1/20 W^A (10 - N^A) N^A$, where N^A is the number of d-electrons and W^A is the width of the d-band. $E_c[BinA]$ is also given as $1/20 W^{BinA} (10 - N^B) N^B$, where $W^{BinA} = (W^B W^A)^{1/2}$ is the d-band width of the solute atom in the host metal. C can be expressed as $C = (1 - (z_I/z_B))^{1/2}$ from the second moment approximation of the density

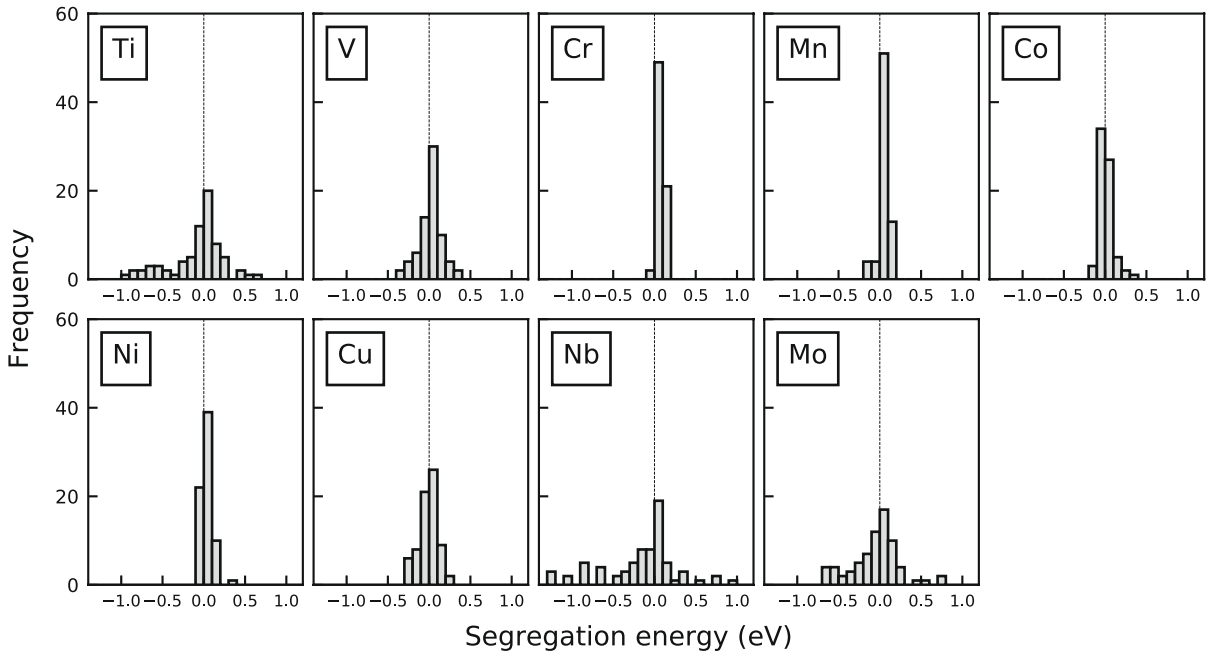

Fig. 4. Histograms of the segregation energy for each element calculated using the nine grain boundary models.

of states, where z_I and z_B are the coordination numbers at the grain boundary and bulk site, respectively.

The phenomenological model of the elastic contribution to the grain boundary segregation energy was obtained by modifying the equation proposed for surface segregation [51–54]. The elastic contribution to the grain boundary segregation energy, E^e_{seg}, is expressed as follows:

$$E^e_{seg} = -\frac{2G_AK_B(V_A - V_B)^2}{4G_AV_B + 3K_BV_A} + \frac{2G_AK_B\left(V^{gb}_A - V_B\right)^2}{4G_AV_B + 3K_BV^{gb}_A} - \frac{2G_AK_A\left(V^{gb}_A - V_A\right)^2}{4G_AV_A + 3K_AV^{gb}_A} \quad (6)$$

Note that a negative value of E^e_{seg} indicates that the elastic energy promotes segregation. V_A and V_B are the atomic volumes of the host metal and solute element, respectively; G_A is the shear modulus of the host metal, K_A and K_B are the bulk moduli of the host metal and solute element, respectively; and V^{gb}_A is the atomic volume of the host metal at the grain boundary site. The first term represents the elastic energy decreased when the solute element in the bulk is removed. The second term represents the increase in elastic energy that occurs when the solute is placed at the segregation site. The third term represents the elastic energy when the host atom at the segregation site is removed. In the following, the first, second, and third terms in Eq. (6) are denoted as $-X_B$, $+X_{GB}$, and $-Fe_{GB}$, respectively.

To clarify the physical origin of the grain boundary segregation, we calculated the dependence of the grain boundary segregation energy of each element on the Voronoi volume of the segregation site using Eqs. (5) and (6). In the chemical contribution given by Eq. (5), z_I and z_B are the number of bonds at the grain boundary and in the bulk, respectively, which are difficult to determine exactly. Scheiber et al. [54] used $z_I/z_B = 11/12$. On the other hand, Geng et al. [55] used $z_I/z_B = 3/4$ for surface segregation, but $z_I/z_B = 1$ for grain boundaries. In other words, Geng et al. considered only the elastic contribution with $C = 0$ at the grain boundaries. In this study, we used both the Scheiber et al. [54] method, in which the elastic and chemical contributions are calculated as $z_I/z_B = 11/12$, and the Geng et al. [55] method, in which only the elastic contribution is considered, for comparison. In this study, the Voronoi volume of Fe at the segregation site was defined as V^{gb}_A, and the dependence of the grain boundary segregation energy of each element on the Voronoi volume at the segregation site was calculated. The parameters for the solute elements in Eqs. (5) and (6) were taken from the same literature values [47] as in Scheiber et al. [54]. Because there are no experimental values for the parameters of the host metal, AFMD γFe, the parameters for the host metal obtained by first-principles calculations were used [56].

Fig. 3 shows the sum of the chemical and elastic contributions to the segregation energy obtained using Eqs. (5) and (6), respectively. The case where $C = 0$, i.e., only the elastic contribution is considered, is shown by the solid line. The segregation energies of the elements calculated by considering only the elastic contribution can effectively reproduce the results of the first-principles calculations. On the other hand, when the chemical contribution is considered, the agreement is worse than when only the elastic contribution is considered. In particular, the segregation energies calculated from first principles are close to zero for all elements when the Voronoi volume is similar to that of the bulk, whereas they have finite values when the chemical contribution is also considered. This indicates that the values of C or z_I/z_B are not appropriate. In general, when the Voronoi volume of a segregation site is close to that of the bulk, the bond number of the segregation site is also close to that of the bulk. Appropriate determination of C depending on the segregation site may provide better agreement with first-principles calculations. Nevertheless, Fig. 3 shows that the main contribution to the segregation energy is the elastic contribution.

Fig. 5 shows the total elastic contribution, E^e_{seg}, and the individual contributions of each term in Eq. (6). In Fig. 5, the first, second, and third terms in Eq. (6) are denoted as $-X_B$, $+X_{GB}$, and $-Fe_{GB}$, respectively. The results show that the contribution of the third term to E^e_{seg} is small in the region of Voronoi volume up to approximately 13 Å, and the first and second terms are dominant. This means that when transition metal elements with atomic volumes different from that of Fe are present in the bulk, extra elastic energy is created. In contrast, transition metal elements with larger atomic volumes can segregate to sites with larger Voronoi volumes, thereby reducing the elastic energy, which in turn leads to a larger negative segregation energy for those sites. On the other hand, in the region where the Voronoi volume is greater than 13 Å, in addition to the above effects, the third term, i.e., the elastic energy decreased when the host atom in the segregation site is removed, also contributes to E^e_{seg}. Thus, the grain boundary segregation energy of the transition metal elements in γFe is dominated by the Voronoi volume of Fe at the segregation site. Moreover, the segregation energy of transition

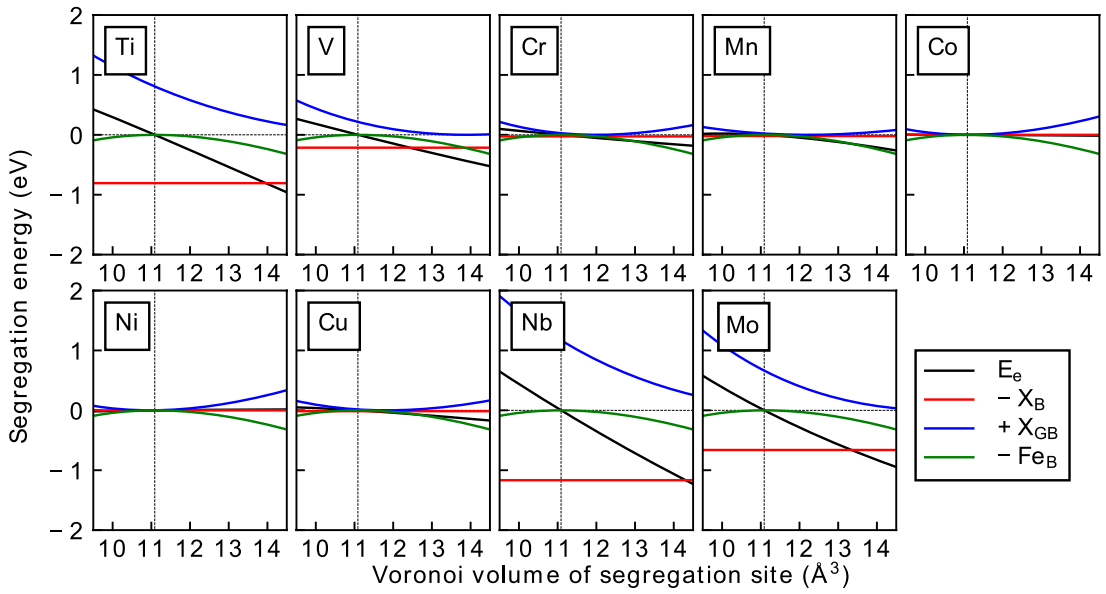

Fig. 5. Relationship between the elastic contribution in the phenomenological model and the Voronoi volume of Fe at the segregation site. The black solid line represents the total elastic contribution, and the red, blue, and green solid lines represent the individual contributions of the first, second, and third terms in Eq. (6). The first, second, and third terms in Eq. (6) are denoted as $-X_B$, $+X_{GB}$, and $-Fe_{GB}$, respectively.

metal elements at each site is mainly determined by the elastic contribution in the phenomenological model of grain boundary segregation.

Here, we discuss this relationship based on the analysis of the Σ3 (1 1 1) grain boundaries and (1 1 1) surfaces of Mo and W by Scheiber et al. [54]. Scheiber et al. [54] calculated the segregation energies of 3d, 4d, and 5d transition metals at the looser site of the Σ3(1 1 1) grain boundary and the (1 1 1) surface in Mo and W. The elastic and chemical contributions were calculated using the phenomenological model described above and compared with the results of first-principles calculations. The surface segregation energies calculated using the phenomenological model reproduced the first-principles results well. On the other hand, the grain boundary segregation energies calculated using the phenomenological model could not effectively reproduce the results of the first-principles calculations. In this case, the chemical contribution is calculated with $z_I/z_B = 11/12$ in Eq. (5) as described above, and then V_A^{gb} for the elastic energy in Eq. (6) is determined by fitting to best reproduce the results of the first-principles calculation. The good reproducibility of the surface segregation energy in W and Mo and of the grain boundary segregation energy in γFe by the phenomenological model suggests that the grain boundary segregation energy in W and Mo can also be reproduced by the phenomenological model through an appropriate treatment of z_I/z_B in the chemical contribution.

3.2. Dependence of effective segregation energy on grain boundary character and comparison with experimental results

In this section, we discuss the segregation tendency of each element and its dependence on the grain boundary character based on the effective segregation energies obtained for each grain boundary model. The calculated results are compared with experimental results to verify the validity.

The dependence of the effective segregation energy of each element on the grain boundary character for $c_{bulk} = 0.0001$ (0.01 at.%) at $T = 1173$ K is shown in Fig. 6. Here, c_{bulk} was set to 0.01 at.% as the bulk composition where carbide-forming elements such as Nb and Ti can remain in the solid solution even in the presence of C. Ti, Cu, Nb, and Mo have negative effective segregation energies at all grain boundaries. For example, the effective segregation energies of Ti, Nb, and Mo in the Σ5 (3 1 0) grain boundary are −0.56, −0.71, and −0.37 eV, respectively. These effective segregation energies indicate that when the solid

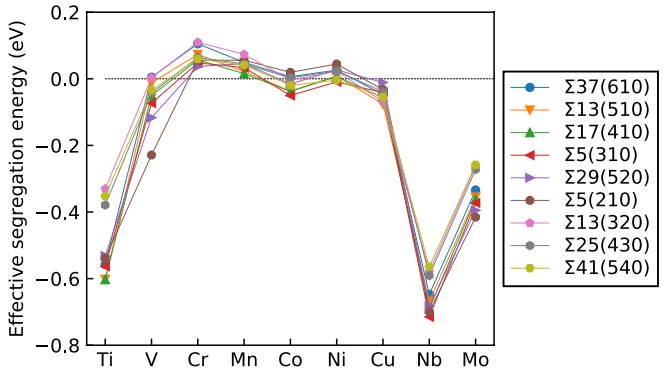

Fig. 6. Effective segregation energy of each element and its dependence on the grain boundary character.

solution amount of each element is 0.01 at.% and the temperature is 1173 K, the segregation amounts of Ti, Nb, and Mo are 2.56 at.%, 10.54 at.%, and 0.40 at.%, respectively, indicating that these elements all have a high segregation tendency. The order of the absolute values of effective segregation energy of these elements is the same for all grain boundary models: Cu < Mo < Ti < Nb. On the other hand, the sign of the effective segregation energy for V, Ni, and Co changes depending on the grain boundary, and the effective segregation energy for Cr and Mn is positive at all grain boundaries, especially for Cr, which shows the most negative segregation tendency among the elements calculated. As mentioned in the previous section, the segregation energy of transition metal elements at each site is effectively described by the Voronoi volume. Because the effective segregation energy in each grain boundary model was calculated using Eqs. (2), (3), and (4), the Voronoi volume of the grain boundary site in each grain boundary model is the dominant factor for the effective segregation energy or the amount of grain boundary segregation.

In this section, we discuss the grain boundary segregation tendency at general grain boundaries. As discussed in the previous section, the segregation energies of the elements calculated in this study are mainly determined by the Voronoi volume. In particular, Nb, Mo, and Ti, which have a high tendency to segregate at grain boundaries, show highly

negative segregation energies at sites with large Voronoi volumes, and this dominates the effective segregation energy. In general, there are always sites where the Voronoi volume is larger than that of the bulk, and the results in Fig. 3 show that the absolute values of segregation energy at these sites are in the order of Mo < Ti < Nb. Therefore, it is reasonable to assume that for the elements with particularly high segregation tendencies, the magnitude of the grain boundary segregation tendency will not change even at the general grain boundary.

In order to verify the validity of the calculation results, we compare the obtained effective segregation energy for the symmetric tilt grain boundaries with the experimental results of segregation energy for general grain boundaries. As mentioned above, there are few experimental results of grain boundary segregation in γFe. The only data that can be compared quantitatively is the segregation energy of Mo and Mn at the prior γ grain boundary investigated by Takahashi et al. using atom probe tomography[57]. Takahashi et al. [57] showed that the segregation energy of Mo for the γFe grain boundary is −0.28 eV at 1223 K with c_{bulk} = 0.3 at.%, and that Mn does not segregate at the γFe grain boundary at 1223 K with c_{bulk} = 1.3 at.%. The effective segregation energies of Mo in the presently calculated grain boundary models under these experimental conditions are in the range of −0.23 to −0.39 eV, which corresponds well with the experimental results. The effective segregation energies of Mn are also small and positive in all the grain boundary models calculated in this study, which is in good agreement with the experimental results. Although quantitative evaluation of the segregation energy was not been performed, Yoo et al. [5] also investigated the grain boundary segregation at γ-grain boundaries of martensitic steels containing Mo and Mn using atom probe tomography, and showed that Mo segregates significantly at γFe grain boundaries, while Mn does not segregate at γFe grain boundaries. Thus, the calculated results correspond well with the comparable experimental results. This suggests that the calculated effective segregation energies of the other alloying elements also reproduce the experimental results well. The results of the segregation energy calculations are summarized in Table S1. Using these segregation energies and equations (2)-(4), it is possible to calculate the amount of segregation and the effective segregation energy depending on the bulk composition and temperature. Recently, it has been shown that the experimental segregation energies of solute elements for general grain boundaries in αFe can be predicted quantitatively by using a nanopolycrystalline grain boundary model that simulates polycrystalline grain boundaries [37,38]. If this method can be applied to γFe in the future, more precise predictions will be possible.

3.3. Validity of using the AFMD to analyze the grain boundary segregation in paramagnetic γFe

In this section, we discuss the validity of using the magnetic structure of the AFMD to analyze the grain boundary segregation in paramagnetic γFe. As shown in Section 3.1, the grain boundary segregation energies of transition metal elements in γFe calculated using the magnetic states of AFMD were effectively explained by the elastic contributions in the phenomenological model. The atomic volume in the magnetic state used as an approximation is important because the dependence of the segregation energy of each alloying element on the Voronoi volume is mainly determined by the atomic volume of the host metal (γFe) and the solute elements, as indicated by Eq. (6). As described in Section 2.1, the lattice parameter (or atomic volume) of γFe under the AFMD magnetic state is similar to that of paramagnetic γFe [29]. Furthermore, a recent study by Sun et al. [56] showed that the elastic properties of γFe under the AFMD magnetic structure best represent those of paramagnetic γFe. Thus, the AFMD magnetic state is a reasonable approximation to account for the elastic contribution, which is particularly important in the calculation of the grain boundary segregation energy of transition metals in γFe.

Next, we discuss the bonding state of Fe with the solute elements in γFe. The magnetic moments of each transition metal element in the bulk AFMD γFe are shown in Fig. 7. To discuss the effect of varying Voronoi volumes of segregation sites on the binding state of solute elements and Fe, the magnetic moments of each transition metal element are shown at sites with particularly large and small Voronoi volumes, i.e., sites with Voronoi volumes of 14.04 Å^3 and 10.68 Å^3 (referred to as looser and tighter sites, respectively). Both sites are in the Σ41(540) grain boundary model. For comparison, we also show the magnetic moments of each transition metal element in the bulk γFe in the magnetic structure using the SQS calculated by Jin et al. [24]. In the calculation by Jin, the SQS structure consisting of 32 atoms was used, and the calculation was performed when one Fe with a positive magnetic moment was replaced with each alloying element. The magnetic moments of each transition metal element in the bulk AFMD γFe in the present calculation are in good agreement with those in the magnetic structure using SQS, indicating that AFMD γFe can effectively reproduce the binding states of Fe and solute elements in the bulk paramagnetic γFe. For Co, a number of calculations were performed by varying the initial magnetic moment and k-point spacing, but the magnetic moment of Co after structural relaxation was negative in all cases. On the other hand, we confirmed that the magnetic moment of Co before structural relaxation can be positive. These results show that the energies of the system are very similar when the magnetic moment of Co is positive and negative in AFMD γFe.

Comparing the magnetic moments at the tighter and looser sites in Fig. 7 with those in the bulk, the magnetic moments of Ti, Ni, Cu, Nb, and Mo are small and almost unchanged between the bulk site and the tighter and looser sites. On the other hand, the absolute values of the magnetic moments of V, Cr, Mn, and Co are larger at the looser site than at the tighter and bulk sites. The same behavior has been reported for αFe [20]. For these elements, the d-d orbital hybridization with neighboring Fe, which is weakened when present at the looser site, is compensated by a larger exchange splitting, resulting in a larger magnetic moment [58,59]. These results suggest that AFMD γFe can properly handle the change in electronic state related to the binding of solute elements to neighboring Fe as a function of the Voronoi volume, which is a determinant of the grain boundary segregation energy.

Thus, AFMD is a good magnetic structure for investigating the grain boundary segregation of transition metal elements in paramagnetic γFe. The above discussion applies not only to grain boundaries, but also to the interaction between solute elements and lattice defects such as dislocations and solute–solute interactions in paramagnetic γFe. Therefore,

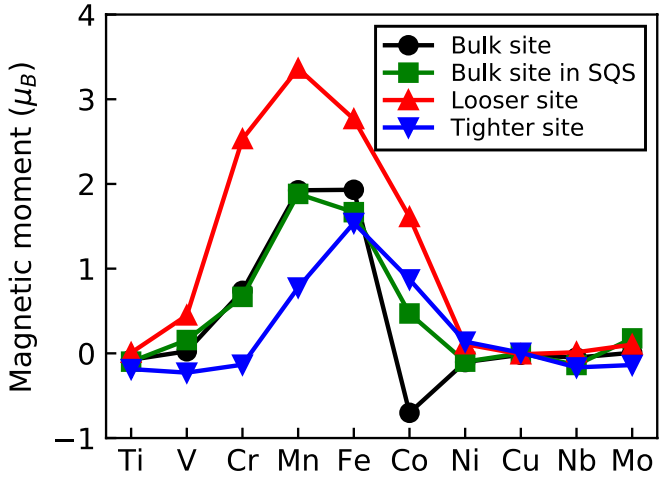

Fig. 7. Magnetic moments of each alloying element in the bulk γFe with the AFMD magnetic structure or magnetic structure created using SQS. The magnetic moments of each alloying element segregated at the looser and tighter sites of the grain boundary model of γFe with the AFMD magnetic structure are also shown.

AFMD is a good approximation for investigating the effect of solute elements in paramagnetic γFe using first-principles calculations.

3.4. Differences in the grain boundary segregation behavior of transition metal elements in αFe and γFe

In this section, we discuss the difference in grain boundary segregation behavior between ferromagnetic αFe and γFe. There are some studies on grain boundary segregation of various solute elements at symmetric tilt grain boundaries in αFe. Jin et al. calculated the grain boundary segregation energies of Si, V, Cr, Mn, Co, Ni, Cu, Ti, Nb, and Mo at Σ5(3 1 0) grain boundaries and showed that the segregation energy of each solute element correlates well with the atomic volume of the solute atom [19]. Based on this result, the importance of elastic energy in the grain boundary segregation energy is highlighted. The bulk modulus and shear modulus are 189 GPa and 83 GPa, respectively for αFe [60], which are not significantly different from the 205 GPa and 81 GPa for γFe [56]. Therefore, based on Eq. (6), which represents the elastic contribution of the phenomenological model, it can be suggested that although there are quantitative changes originating from the bulk modulus and shear modulus between αFe and γFe, the qualitative behaviors, such as the large and small grain boundary segregation for Ti, V, Cu, Nb, and Mo with large atomic volumes, are similar in the two phases. On the other hand, chemical contributions also play an important role in the grain boundary segregation of elements with small atomic volumes. As one form of chemical contribution, the difference in binding between Fe and solute elements due to the difference in magnetism between the two phases may qualitatively affect the segregation behavior. For example, in αFe, it has been shown that Mn has a segregation energy negatively higher than −0.2 eV at looser and tighter sites at the Σ3(1 1 1) and Σ11(3 3 2) grain boundaries [20]. It is also known experimentally that Mn segregates at grain boundaries in αFe polycrystals [36]. On the other hand, as mentioned above, in γFe, the present calculations and experimental results [5,57] show that Mn has almost no tendency to segregate at grain boundaries. We have shown that the segregation energy of Mn at the looser site in the Σ3(1 1 1) grain boundary of αFe is large (−0.49 eV) in the case of antiferromagnetic coupling with the surrounding Fe, while it is small (−0.07 eV) at the same site in the case of metastable ferromagnetic coupling Mn [22]. In addition, Xu et al. analyzed the electric origin of grain boundary segregation of Mn at Σ3 (1 1 1) and Σ11(3 3 2) grain boundaries in αFe in detail based on *ab initio* local energy analysis [20]. It was shown that the antiferromagnetic binding of Mn in the bulk greatly increased the energy of the surrounding Fe atoms, but this energy increase was smaller at grain boundaries, resulting in a negatively large grain boundary segregation energy. These results suggest that the difference in the segregation behavior of Mn between αFe and γFe is related to the difference in the magnetic states of the two phases. For an element with such a small elastic contribution, the difference in the magnetic state between αFe and γFe may cause a qualitative change in the segregation behavior. This needs to be investigated in more detail by systematic analysis of the grain boundary segregation tendency of each element in αFe and its effect on the grain boundary character, and by application of local energy analysis [18,20,21] to the grain boundary segregation in γFe. The magnetic structure of the AFMD used in this study reproduces the experimental results of the grain boundary segregation tendency of Mn in γFe, indicating the validity of the magnetic structure of the AFMD.

4. Conclusion

We proposed a magnetic state and a data set of grain boundary models for the systematic investigation of grain boundary segregation in paramagnetic γFe through first-principles calculations. The segregation energies of nine transition metal alloying elements (Ti, V, Cr, Mn, Co, Ni, Cu, Nb, and Mo) commonly used in steel materials were comprehensively calculated. The segregation energy of transition metal elements was found to be dominated by the Voronoi volume of Fe at clean grain boundaries without solute elements at the segregation site. Based on the obtained segregation energies and the phenomenological model of grain boundary segregation, the physical origin of the grain boundary segregation was discussed, and it was shown that the segregation energy of each element could be effectively explained by the elastic energy derived from the difference in atomic radii between the host metal and solute element.

In addition, the tendency of each alloying element to segregate at grain boundaries and the dependence on the grain boundary character were investigated by calculating the effective segregation energy for each grain boundary model. Ti, Cu, Nb, and Mo showed negative effective segregation energies at all calculated grain boundaries and had a high tendency to segregate at the grain boundaries. The order of the absolute values of the effective segregation energy of these elements was the same for all grain boundary models, Cu < Mo < Ti < Nb, suggesting that the order of the effective segregation energies are the same for the general grain boundaries. On the other hand, the sign of the effective segregation energies for V, Ni, and Co changed depending on the grain boundary, and the effective segregation energies for Cr and Mn were positive at all grain boundaries, particularly for Cr, which exhibited the most negative segregation tendency among the elements considered. These results corresponded well with the experimental results. The AFMD magnetic structure could effectively reproduce the lattice parameter and elastic modulus of paramagnetic γFe, as well as the bonding state between transition metal elements and Fe. These results indicate that AFMD is a good approximation for investigating not only grain boundary segregation but also the effect of alloying elements in γFe using first-principles calculations.

The results obtained in this study provide important basic data for the material design of high-strength steels and are useful for understanding the effects of alloying elements in γFe.

5. Data statement

The raw/processed data required to reproduce these findings cannot be shared at this time as the data also forms part of an ongoing study.

CRediT authorship contribution statement

Kazuma Ito: Conceptualization, Methodology, Software, Data curation, Writing – original draft, Visualization, Investigation. **Hideaki Sawada:** Supervision, Validation, Writing – review & editing.

Declaration of Competing Interest

The authors declare that they have no known competing financial interests or personal relationships that could have appeared to influence the work reported in this paper.

Appendix A. Supplementary material

Supplementary data to this article can be found online at https://doi.org/10.1016/j.commatsci.2021.111050.

References

[1] C.D. Horvath, Chapter 2 - Advanced steels for lightweight automotive structures, in: P.K. Mallick (Ed.), Materials, Design and Manufacturing for Lightweight Vehicles (Second Edition), Woodhead Publishing, Cambridge, 2021, pp. 39–95.
[2] D.-W. Suh, S.-J. Kim, Medium Mn transformation-induced plasticity steels: recent progress and challenges, Scr. Mater. 126 (2017) 63–67.
[3] R.L. Plaut, C. Herrera, D.M. Escriba, P.R. Rios, A.F. Padilha, A short review on wrought austenitic stainless steels at high temperatures: processing, microstructure, properties and performance, Mater. Res 10 (4) (2007) 453–460.
[4] D.V. Edmonds, K. He, F.C. Rizzo, B.C. De Cooman, D.K. Matlock, J.G. Speer, Quenching and partitioning martensite—A novel steel heat treatment, Mater. Sci. Eng., A 438–440 (2006) 25–34.

[5] J. Yoo, M.C. Jo, M.C. Jo, S. Kim, S.-H. Kim, J. Oh, S.S. Sohn, S. Lee, Effects of solid solution and grain-boundary segregation of Mo on hydrogen embrittlement in 32MnB5 hot-stamping steels, Acta Mater. 207 (2021), 116661.
[6] M. Soleimani, A. Kalhor, H. Mirzadeh, Transformation-induced plasticity (TRIP) in advanced steels: a review, Mater. Sci. Eng., A 795 (2020) 140023, https://doi.org/10.1016/j.msea.2020.140023.
[7] J.P. Hirth, Effects of hydrogen on the properties of iron and steel, Metall. Trans. A 11 (6) (1980) 861–890.
[8] D. Hardie, S.E. Liu, The effect of stress concentration on hydrogen embrittlement of a low alloy steel, Corros. Sci. 38 (5) (1996) 721–733.
[9] L.W. Tsay, M.Y. Chi, Y.F. Wu, J.K. Wu, D.-Y. Lin, Hydrogen embrittlement susceptibility and permeability of two ultra-high strength steels, Corros. Sci. 48 (8) (2006) 1926–1938.
[10] M.C. Jo, J. Yoo, S. Kim, S. Kim, J. Oh, J. Bian, S.S. Sohn, S. Lee, Effects of Nb and Mo alloying on resistance to hydrogen embrittlement in 1.9 GPa-grade hot-stamping steels, Mater. Sci. Eng., A 789 (2020), 139656.
[11] H. Mohrbacher, T. Senuma, Alloy optimization for reducing delayed fracture sensitivity of 2000 MPa press hardening steel, Metals 10 (7) (2020) 853–871.
[12] P. Lejček, Grain Boundary Segregation in Metals, Springer Science & Business Media, Springer-Verlag, Berlin, 2010.
[13] M. Yamaguchi, Y. Nishiyama, H. Kaburaki, Decohesion of iron grain boundaries by sulfur or phosphorous segregation: first-principles calculations, Phys. Rev. B 76 (3) (2007), 035418.
[14] M. Čák, M. Šob, J. Hafner, First-principles study of magnetism at grain boundaries in iron and nickel, Phys. Rev. B 78 (5) (2008), 054418.
[15] E. Wachowicz, A. Kiejna, Effect of impurities on structural, cohesive and magnetic properties of grain boundaries in α-Fe, Model. Simul. Mat. Sci. Eng. 19 (2) (2011) 025001, https://doi.org/10.1088/0965-0393/19/2/025001.
[16] M. Yamaguchi, First-principles study on the grain boundary embrittlement of metals by solute segregation: Part I. Iron (Fe)-solute (B, C, P, and S) systems, Metall. Mater. Trans. A 42 (2) (2011) 319–329.
[17] M. Yamaguchi, K.-I. Ebihara, M. Itakura, T. Kadoyoshi, T. Suzudo, H. Kaburaki, First-principles study on the grain boundary embrittlement of metals by solute segregation: Part II. Metal (Fe, Al, Cu)-hydrogen (H) systems, Metall. Mater. Trans. A 42 (2) (2011) 330–339.
[18] S.K. Bhattacharya, M. Kohyama, S. Tanaka, Y. Shiihara, Si segregation at Fe grain boundaries analyzed by ab initio local energy and local stress, J. Phys.: Condens. Matter 26 (35) (2014) 355005, https://doi.org/10.1088/0953-8984/26/35/355005.
[19] H. Jin, I. Elfimov, M. Militzer, Study of the interaction of solutes with Σ5 (013) tilt grain boundaries in iron using density-functional theory, J. Appl. Phys. 115 (9) (2014) 093506, https://doi.org/10.1063/1.4867400.
[20] Z. Xu, S. Tanaka, M. Kohyama, Grain-boundary segregation of 3d-transition metal solutes in bcc Fe: Ab initio local-energy and d-electron behavior analysis, J. Phys.: Condens. Matter 31 (11) (2019), 115001.
[21] K. Ito, H. Sawada, S. Tanaka, S. Ogata, M. Kohyama, Electronic origin of grain boundary segregation of Al, Si, P, and S in bcc-Fe: combined analysis of ab initio local energy and crystal orbital Hamilton population, Model. Simul. Mat. Sci. Eng. 29 (1) (2020), 015001.
[22] K. Ito, H. Sawada, S. Ogata, First-principles study on the grain boundary embrittlement of bcc-Fe by Mn segregation, Phys. Rev. Mater. 3 (1) (2019), 013609.
[23] M. Yuasa, M. Mabuchi, First-principles study in Fe grain boundary with Al segregation: variation in electronic structures with straining, Philos. Mag. 93 (6) (2013) 635–647.
[24] H. Jin, Atomistic Simulations of Solute-Interface Interactions in Iron, University of British Columbia, 2014.
[25] A. Zunger, S.-H. Wei, L.G. Ferreira, J.E. Bernard, Special quasirandom structures, Phys. Rev. Lett. 65 (3) (1990) 353–356.
[26] A.V. Ponomareva, Y.N. Gornostyrev, I.A. Abrikosov, Ab initio calculation of the solution enthalpies of substitutional and interstitial impurities in paramagnetic fcc Fe, Phys. Rev. B 90 (1) (2014), 014439.
[27] D.W. Boukhvalov, Y.N. Gornostyrev, M.I. Katsnelson, A.I. Lichtenstein, Magnetism and local distortions near carbon impurity in $\ensuremath{\gamma}$-Iron, Phys. Rev. Lett. 99 (24) (2007), 247205.
[28] N.I. Medvedeva, D. Van Aken, J.E. Medvedeva, Magnetism in bcc and fcc Fe with carbon and manganese, J. Phys.: Condens. Matter 22 (31) (2010) 316002, https://doi.org/10.1088/0953-8984/22/31/316002.
[29] D.E. Jiang, E.A. Carter, Carbon dissolution and diffusion in ferrite and austenite from first principles, Phys. Rev. B 67 (21) (2003), 214103.
[30] M.A. Tschopp, S.P. Coleman, D.L. McDowell, Symmetric and asymmetric tilt grain boundary structure and energy in Cu and Al (and transferability to other fcc metals), Integr. Mater. Manuf. Innov. 4 (1) (2015) 176–189.
[31] D. Scheiber, R. Pippan, P. Puschnig, L. Romaner, Ab initiocalculations of grain boundaries in bcc metals, Model. Simul. Mat. Sci. Eng. 24 (3) (2016) 035013, https://doi.org/10.1088/0965-0393/24/3/035013.
[32] Q. Zhu, A. Samanta, B. Li, R.E. Rudd, T. Frolov, Predicting phase behavior of grain boundaries with evolutionary search and machine learning, Nat. Commun. 9 (1) (2018) 467.
[33] S. Divinski, M. Lohmann, C. Herzig, Ag grain boundary diffusion and segregation in Cu: measurements in the types B and C diffusion regimes, Acta Mater. 49 (2) (2001) 249–261.
[34] J. Sommer, Chr. Herzig, Direct determination of grain-boundary and dislocation self-diffusion coefficients in silver from experiments in type-C kinetics, J. Appl. Phys. 72 (7) (1992) 2758–2766.
[35] K. Hirokawa, S. Suzuki, K. Abiko, H. Kimura, M. Oku, Estimation of the thickness or composition of a covering layer on a solid by XPS or AES, J. Electron Spectros. Relat. Phenomena 24 (2) (1981) 243–253.
[36] M. Guttmann, Ph. Dumoulin, M. Wayman, The thermodynamics of interactive co-segregation of phosphorus and alloying elements in iron and temper-brittle steels, Metall. Trans. A 13 (10) (1982) 1693–1711.
[37] K. Ito, H. Sawada, S. Ogata, Theoretical prediction of grain boundary segregation using nano-polycrystalline grain boundary model, Mater. Trans. 62 (5) (2021) 575–581.
[38] K. Ito, H. Sawada, S. Ogata, Theoretical prediction of grain boundary segregation using nano-polycrystalline grain boundary model, J. Japan Inst. Met. Mater. 84 (7) (2020) 237–243.
[39] G. Kresse, J. Furthmüller, Efficient iterative schemes for ab initio total-energy calculations using a plane-wave basis set, Phys. Rev. B 54 (16) (1996) 11169–11186.
[40] G. Kresse, D. Joubert, From ultrasoft pseudopotentials to the projector augmented-wave method, Phys. Rev. B 59 (3) (1999) 1758–1775.
[41] J.P. Perdew, K. Burke, M. Ernzerhof, Generalized gradient approximation made simple, Phys. Rev. Lett. 77 (18) (1996) 3865–3868.
[42] H.J. Monkhorst, J.D. Pack, Special points for Brillouin-zone integrations, Phys. Rev. B 13 (12) (1976) 5188–5192.
[43] R. Iglesias, S. Palacios, Ab initio studies on the magnetic phase stability of iron, Acta Mater. 55 (15) (2007) 5123–5127.
[44] H. Jin, I. Elfimov, M. Militzer, First-principles simulations of binding energies of alloying elements to the ferrite-austenite interface in iron, J. Appl. Phys. 123 (8) (2018) 085303, https://doi.org/10.1063/1.5020166.
[45] C.L. White, W.A. Coghlan, The spectrum of binding energies approach to grain boundary segregation, Metall. Trans. A 8 (9) (1977) 1403–1412.
[46] D. McLean, Grain Boundary Segregation in Metals, Clarendon Press, Oxford, 1957.
[47] H. Bakker, Enthalpies in Alloys, Trans Tech Publ, 1998.
[48] A.V. Ruban, H.L. Skriver, J.K. Nørskov, Surface segregation energies in transition-metal alloys, Phys. Rev. B 59 (24) (1999) 15990–16000.
[49] H.A. Murdoch, C.A. Schuh, Estimation of grain boundary segregation enthalpy and its role in stable nanocrystalline alloy design, J. Mater. Res. 28 (16) (2013) 2154–2163.
[50] J. Friedel, The physics of clean metal surfaces, Ann. Phys. 1 (1976) 257–307.
[51] J.D. Eshelby, Distortion of a crystal by point imperfections, J. Appl. Phys. 25 (2) (1954) 255–261.
[52] J. Friedel, Electronic structure of primary solid solutions in metals, Adv. Phys. 3 (12) (1954) 446–507.
[53] J.D. Eshelby, The continuum theory of lattice defects, Solid State Phys. 3 (1956) 79–144.
[54] D. Scheiber, R. Pippan, P. Puschnig, A. Ruban, L. Romaner, Ab-initio search for cohesion-enhancing solute elements at grain boundaries in molybdenum and tungsten, Int. J. Refract. Met. Hard Mater. 60 (2016) 75–81.
[55] W.T. Geng, A.J. Freeman, G.B. Olson, Influence of alloying additions on grain boundary cohesion of transition metals: first-principles determination and its phenomenological extension, Phys. Rev. B 63 (16) (2001), 165415.
[56] L. Sun, H.R. Gong, X. Gong, Magnetic ground state of face-centered-cubic structure of iron, J. Phys.: Condens. Matter 32 (16) (2020) 165806, https://doi.org/10.1088/1361-648X/ab6869.
[57] J. Takahashi, K. Ishikawa, K. Kawakami, M. Fujioka, N. Kubota, Atomic-scale study on segregation behavior at austenite grain boundaries in boron- and molybdenum-added steels, Acta Mater. 133 (2017) 41–54.
[58] J. Kübler, Theory of Itinerant Electron Magnetism, Oxford University Press, Oxford, 2017.
[59] L. Zhang, M. Šob, Z. Wu, Y. Zhang, G.-H. Lu, Characterization of iron ferromagnetism by the local atomic volume: from three-dimensional structures to isolated atoms, J. Phys.: Condens. Matter 26 (8) (2014), 086002.
[60] M. Souissi, H. Numakura, Elastic properties of Fe–C and Fe–N martensites, ISIJ Int. 55 (7) (2015) 1512–1521.